Journal of Materials Chemistry C

Effect of Quantum Tunneling on the Efficiency of Excitation Energy Transfer in Plasmonic Nanoparticle Chain Waveguides

Journal:	*Journal of Materials Chemistry C*
Manuscript ID	TC-ART-03-2018-001466.R1
Article Type:	Paper
Date Submitted by the Author:	07-May-2018
Complete List of Authors:	Ilawe, Niranjan; University of California, Riverside, Department of Chemical & Environmental Engineering Oviedo, Maria Belen; University of California, Riverside, Department of Chemical & Environmental Engineering Wong, Bryan; University of California-Riverside, Chemical & Environmental Engineering and Materials Science & Engineering

SCHOLARONE™
Manuscripts

Journal Name

Effect of quantum tunneling on the efficiency of excitation energy transfer in plasmonic nanoparticle chain waveguides

Niranjan V. Ilawe,[a] M. Belén Oviedo,[b,c] and Bryan M. Wong[*a]

We present a detailed analysis of the electronic couplings that mediate excitation energy transfer (EET) in plasmonic nanoantenna systems using large-scale quantum dynamical calculations. To capture the intricate electronic interactions in these large systems, we utilize a real-time, time-dependent, density functional tight binding (RT-TDDFTB) approach to characterize the quantum-mechanical efficiency of EET in plasmonic nanoparticle chains with subnanometer interparticle spacings. In contrast to classical electrodynamics methods, our quantum dynamical calculations do not predict a monotonic increase in EET efficiency with a decrease in interparticle spacing between the nanoparticles of the nanoantenna. Most notably, we show a sudden drop in EET efficiencies as the interparticle distance approaches subnanometer length scales within the nanoparticle chain. We attribute this drop in EET efficiency to the onset of quantum charge tunneling between the nanoparticles of the chain which, in turn, changes the nature of the electronic couplings between them. We further characterize this abrupt change in EET efficiency through visualizations of both the spatial and time-dependent charge distributions within the nanoantenna, which provide an intuitive classification of the various types of electronic excitations in these plasmonic systems. Finally, while the use of classical electrodynamics methods have long been used to characterize complex plasmonic systems, our findings demonstrate that quantum-mechanical effects can result in qualitatively different (and sometimes completely opposite) results that are essential for accurately calculating EET mechanisms and efficiencies in these systems.

Achieving a controlled transfer of energy and information at high speeds and minimal losses has been a continual research goal in technological fields ranging from energy harvesting to nanophotonic circuits.[1–4] Coupling light to localized surface plasmon resonances (LSPRs)[5] in metallic nanoparticle ensembles provides an electromagnetic pathway to direct and control this flow of energy. Starting with the ground-breaking experimental demonstration of this phenomena by Maier et al.,[6] many other researchers[7,8] have also shown experimental evidence of other excitation energy transfer (EET) mechanisms. In terms of applications, others have also recently examined waveguides with various shapes such as L-bends,[9] T-joints,[10] Y-splitters,[11] and other more complex ensembles that are inspired from natural light-harvesting antenna systems.[12]

One of the recurring issues with the practical application of these plasmonic ensembles in fields such as photonic circuits and energy harvesting is that the propagation distance of energy remains too short.[6] A possible way for increasing this propagation distance in plasmonic chains is to decrease the interparticle spacings, which results in stronger plasmon couplings.[13–15] Another factor, particularly for applications in photonics circuits, is that the overall size of the electronic components in such circuits has reached subnanometer sizes. This has made it necessary to reduce the size of the transport structures, i.e. the nanoparticle ensembles, to subnanometer sizes.[16] While the production of both smaller interparticle spacings and small nanoparticles were limited with lithographic manufacturing methods, the advent of bottom-up assembly techniques for metallic nanoparticle ensembles have partially solved this problem.[13–15,17,18] This approach is not only cost-effective, but has also made possible the fabrication of complex nanoparticle assemblies with subnanometer interparticle spacings.[19,20]

These nanoscale structures, which are separated by small interparticle gaps, support hybridized plasmon resonances as a re-

[a]Department of Chemical and Environmental Engineering, and Materials Science and Engineering Program, University of California-Riverside, Riverside, CA 92521, USA. E-mail: bryan.wong@ucr.edu; Web: http://www.bmwong-group.com
[b]Universidad Nacional de Córdoba, Facultad de Ciencias Químicas, Departamento de Química Teórica y Computacional, Córdoba, Argentina; E-mail: mboviedo@unc.edu.ar
[c]INFIQC, CONICET, X5000HUA, Córdoba, Argentina

sult of interactions between the basic plasmon resonances of the elementary nanoparticles. For example, the Bonding Dipole hybridized Plasmon (BDP) is characterized by in-phase charge oscillations in each of the nanoparticles.[21] Another hybridized plasmon mode, the Charge Transfer Plasmon (CTP), is observed in the structure when the nanoparticles touch each other or a conductive junction is established between them, allowing for a direct charge transfer from one nanoparticle to the other.[22] The onset of such hybridized plasmon resonances drastically modify the near and far field properties of the systems and has led to increased interest in their applicability in novel devices.[23–29] However, recent studies have shown that as the interparticle spacing enters the subnanometer regime, the quantum nature of the electrons significantly alters the plasmonic response of the system.[22] In particular, in the quantum regime, electrons can tunnel through the flat energy barrier between nanoparticles and thus enable a CTP before the particles touch each other. This is known as direct tunneling. Another form is Fowler-Nordheim tunneling, where tunneling occurs in the presence of high electric fields.[30]

As such, the need to fabricate subnanometer nanoparticle assemblies has posed additional problems for the theoretical analysis of these structures. The most widely employed approaches for analyzing EET in nanoparticle assemblies has been finite-difference time-domain (FDTD) calculations or similar methods based on solving Maxwell's equations. These methods rely on the Drude model to characterize bulk metal properties such as the plasma frequency.[9,31–33] Other approaches have also employed Förster resonance energy transfer (FRET) models to study EET in plasmonic structures,[34–36] but these methodologies contain various approximations, such as the spectral overlap and dipole approximation, which limit their applicability to complex systems.[37–39] Along with these approximations, most of these studies limit their analyses to systems with a minimum interparticle spacing of 1 nm and above.[9,10,31,32,40] Also, as mentioned previously, with smaller dimensions, quantum effects will ultimately play an important role, and it is essential to consider these non-classical effects. Recent studies have begun to address this problem by proposing quantum-corrected models within classical electromagnetic simulations;[41,42] however, these models do not provide an atomistic treatment of the systems under study. While first-principle methods such as DFT can correctly predict quantum effects, the large size of nanoparticle assemblies remain beyond their reach with current computational resources. In this work, we probe in atomistic detail the electronic couplings in metal nanoparticle chains with varying inter-particle spacings using the density functional tight-binding approach and its real-time, time-dependent counterpart, RT-TDDFTB. In contrast to our previous study on long-range EET mechanisms,[39] this study investigates extremely small inter-particle spacings, where quantum effects play an important role and are beyond the scope of classical FDTD methods. Based on our RT-TDDFTB calculations, we reveal two different regimes of EET efficiency: (1) For large inter-particle separations, EET efficiency increases with decreasing inter-particle spacing, which is consistent with classical calculations; (2) a sudden drop in efficiency is observed as the inter-particle distance is further reduced, even before the nanoparticles touch each other.

We attribute this drop in efficiency to the onset of an interparticle charge transfer between the nanoparticles of the chain. We also show that the onset of this charge transfer mechanism in the nanoparticle chain dramatically alters the nature of the coupling between the plasmonic nanoparticles. In particular, the bonding dipole plasmon (BDP) is converted to a hybridized-BDP with some charge transfer character, which is responsible for the decrease in the capacitive coupling in the nanoparticle chain. We also propose a visually intuitive way to classify the peaks in the absorption spectrum of the nanoparticles as various types of plasmonic excitations. While we focus our study on a simple chain-like ensemble of nanoparticles, our methodology is expected to apply to a broad range of other complex plasmonic ensembles.

Theory and Methodology

The real-time electron dynamics for very large systems (at an electronic and atomistic level of detail) cannot be routinely calculated with conventional linear-response TD-DFT or other continuum models. To probe the large nanoparticle assemblies in this work, we utilize the self-consistent density functional tight-binding (SCC-DFTB) formalism along with its real-time, time-dependent counterpart, RT-TDDFTB. This formalism has been previously used to probe the nonequilibrium electron dynamics in several large chemical systems,[43] including photoinjection dynamics in dye-sensitized TiO_2 solar cells,[44,45] many-body interactions in solvated nanodroplets,[46] and long-range couplings in plasmonic nanoantennas.[39] While we give a brief description of the methodology here, a more detailed description on the DFTB and SCC-DFTB formalism can be found in refs 47 and 48.[47,48] DFTB is an application of the tight-binding (TB) approach to parameterize full DFT. The main idea behind this method is to describe the Hamiltonian eigenstates with an atomic-like basis set and replace the Hamiltonian with parameterized matrix elements that depend only on the internuclear distances (neglecting integrals of more than two centers) and orbital symmetries. The origin of DFTB begins with the expression of the Kohn-Sham total energy,

$$E_{KS} = \sum_i^{occ} \langle \psi_i | (-\frac{1}{2}\nabla^2 + V_{ext}) | \psi_i \rangle + E_H + E_{xc} + E_{II} \quad (1)$$

where V_{ext} is the external interaction (including electron-ion interactions), E_H is the Hartree energy, $E_{xc} = (T-T_s) + (E_{ee}-E_H)$ is the exchange-correlation energy and E_{II} is the ion-ion interaction energy. Upon expanding the Kohn-Sham total energy in terms of a reference density and a small correction $\rho_0 + \delta\rho$, the DFTB energy is parameterized as

$$E_{DFTB} = \sum_i^{occ} \langle \varphi_i | \hat{H}_0 | \varphi_i \rangle + \frac{1}{2} \sum_{AB}^{M} \gamma_{AB} \Delta q_A \Delta q_B + E_{rep}^{AB} \quad (2)$$

The first term in eq 2 corresponds to a Kohn-Sham effective Hamiltonian, $\hat{H}_0$, evaluated at the reference density, ρ_0, and is approximated in the DFTB framework as,

$$\hat{H}_0 \approx \langle \varphi_\mu | \hat{T} + v_{eff}[\rho_A^0 + \rho_B^0] | \varphi_\nu \rangle, \mu \in A, \nu \in B \quad (3)$$

where φ_μ forms a minimal Slater-type orbital basis centered on the atomic sites, ρ_A^0 is the reference density of the neutral atom

A, and v_{eff} is the effective Kohn-Sham potential. It should be noted that the Hamiltonian matrix elements depend only on atoms A and B and, therefore, only two-center Hamiltonian matrix elements, as well as two-center elements of the overlap matrix, are explicitly calculated using analytical functions as per the LCAO (linear combination of atomic orbitals) formalism. These matrix elements are pre-tabulated for all pairs of chemical elements as a function of distance between atomic pairs, thus significantly improving the computational efficiency of the DFTB approach. The second term in Eq. 2 is the energy due to charge fluctuations and is parameterized analytically as a function of orbital charges and γ_{AB}, which is a function of inter-atomic separation and the Hubbard parameter (U).[49] The quantity $\Delta q_A = q_A - q_A^0$ is the difference between the charge of the isolated atom q_A^0 and the charge q_A obtained via a Mulliken population analysis of atom A in the molecule. E_{rep} is the distance-dependent diatomic repulsive potential and contains the core electron effects, ion-ion repulsion terms, as well as some exchange-correlation effects. E_{rep} can be considered as a practical equivalent to an xc-functional in DFT as it approximates the many-body correlation interactions with simple functions. As per the consideration of free atoms, ρ_0 is spherically symmetric; hence, the ion-ion repulsion can be approximated to depend only on the elements and their distance. Contributions of 3 and more centers are rather small and can be neglected. These pair-wise repulsive functions are obtained by fitting to DFT calculations using a suitable reference structure. With this assumption of tightly bound electrons and a minimal local basis (only one radial function for each angular momentum state), the DFTB Hamiltonian is given by

$$\hat{H}_{DFTB} = \langle \varphi_\mu | \hat{H}_0 | \varphi_v \rangle + \frac{1}{2} \hat{S}_{\mu v} \sum_X (\gamma_{AX} + \gamma_{BX}) \Delta q_X \qquad (4)$$

where the Hamiltonian matrix elements and the overlap matrix elements are precalculated as discussed above. Since the DFTB Hamiltonian depends explicitly on the atomic charge, a self-consistent charge (SCC) procedure is used in the SCC-DFTB approach to self-consistently solve eq 4.

Once the initial electronic ground state is calculated using the above procedure, it is used as an initial input condition in the real-time quantum dynamics calculations. We carry out our real-time quantum dynamics calculations by applying a time-dependent electric field to the initial ground state density matrix, resulting in the Hamiltonian

$$\hat{H}(t) = \hat{H}^0 - E_0(t) \cdot \hat{\mu}(t) \qquad (5)$$

where $E_0(t)$ is the applied electric field, and $\hat{\mu}$ is the dipole moment operator. As we are directly propagating the quantum system in the time domain, we can choose $E_0(t)$ to have any time-dependent form. For example, if $E_0(t)$ is a Dirac delta function $(= E_0 \delta(t - t_0))$, this corresponds to an optical absorption spectrum in the frequency domain (obtained after a Fourier transform of the time-evolving dipole moment). However, if we choose $E_0(t)$ to take the form of a sinusoidal perturbation, it represents a continuous interaction of the system with monochromatic light in the time domain. Both of these different choices give different but
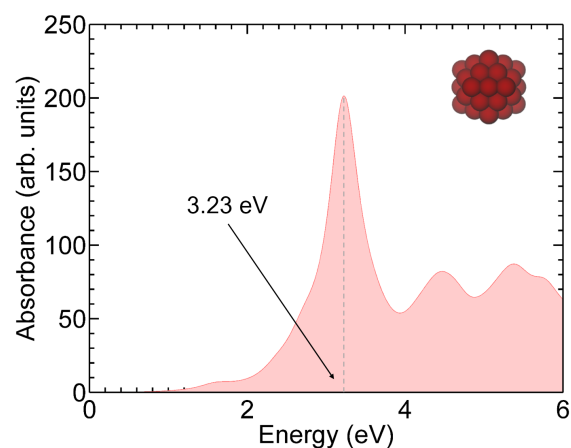

Fig. 1 Absorption spectra of a 55 atom icosahedral silver nanoparticle. A prominent plasmon resonance peak is observed around 3.23 eV.

complementary viewpoints of quantum dynamics. Upon application of either of these time-dependent fields, the density matrix, $\hat{\rho}$, will evolve according to the Liouville-von Neumann equation of motion which, in the nonorthogonal-DFTB basis, is given by

$$\frac{\partial \hat{\rho}}{\partial t} = \frac{1}{i\hbar} (S^{-1} \cdot \hat{H}[\hat{\rho}] \cdot \hat{\rho} - \hat{\rho} \cdot \hat{H}[\hat{\rho}] \cdot S^{-1}) \qquad (6)$$

where $\hat{H}$ is the Hamiltonian matrix (which implicitly depends on the density matrix), S^{-1} is the inverse of the overlap matrix, and $\hbar$ is Planck's constant. When the applied incident fields are smaller than the internal fields within the matter, the system is found to be in the linear response regime.[50] We utilized the DFTB+ code[51] to compute the ground-state Hamiltonian, overlap matrix elements, and the initial single-electron density matrix within the self-consistent DFTB approach.

Results and Discussion

As mentioned previously, the transfer of excitation energy along metal nanoparticle chains takes place via an electromagnetic pathway provided by local surface plasmon resonances. Therefore, we begin the analysis of EET along plasmonic chains by first characterizing the plasmon resonance energy of a single silver NP containing 55 atoms and having an icosahedral shape. Accordingly, we optimize the geometry of the NP and plot its absorption spectrum. We use the hyb-0-2 set of DFTB parameters (available at dftb.org) for computing these properties. As can be seen in Figure 1, a prominent peak, corresponding to the plasmon resonance is observed around 3.23 eV. This result is in good agreement with a time-dependent density functional theory (DFT) calculation of 3.6 eV[52] and a recent experimental result of 3.8 eV[53] for similar-sized Ag nanoparticles.

Along with the absorption spectrum, we also plot the field enhancement of a single Ag NP in Figure 2. Specifically, the Ag NP is excited with a sinusoidal electric field with its frequency equal to its plasmonic energy (3.23 eV) and polarized in the direction of its transition dipole moment. The electric field induced by plasmonic oscillations at any point in space is calculated using the
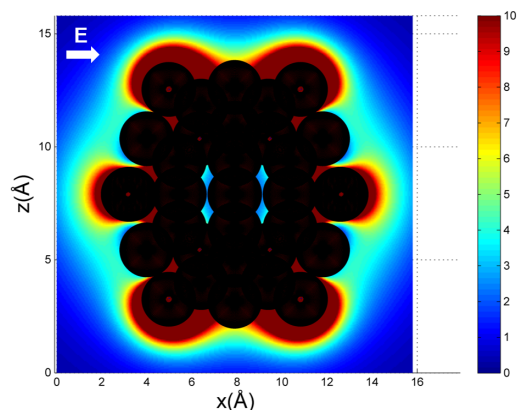
Fig. 2 Electric field enhancement of a Ag_{55} NP exhibiting a dipolar orientation in alignment with the polarization vector **E**. The dark spheres indicate the position of the Ag atoms.

following expression:

$$E(r) = \sum_i \frac{\Delta q_i}{4\pi\varepsilon_0} \frac{(r_i - r)}{||r_i - r||^3} \tag{7}$$

and the electric field enhancement, Γ, is calculated as follows:[54]

$$\Gamma = \frac{|E|^2(\omega)}{|E_{appl}|^2(\omega)} \tag{8}$$

where the applied field has the form $E_{appl}(t) = E_0 \sin(\omega t)$ in the time domain, and ω is the plasmon energy. As expected from plasmonic excitations, high values of field enhancements are observed around the Ag NP, which are distributed in a dipolar fashion, as shown in Figure 2.

Exploring excitation energy transfer in Ag NP chains

With the energy of a single Ag nanoparticle (NP) characterized, we now proceed to an analysis of the EET in plasmonic NP assemblies. Accordingly, we use the single Ag NP to construct model NP chains, each containing 8 Ag NPs and with varying interparticle spacings. As mentioned earlier, previous studies have mostly investigated the EET in NP chains with considerably larger interparticle distances where quantum effects can be safely neglected,[32,55] and approximations such as the dipolar approximation are valid.[39] Here, we are specifically interested in the subnanometer interparticle spacings where both these approximations do not hold. Therefore, we construct model NP chains with interparticle distances (d) varying between 5 Å to 0.5 Å. We define the interparticle distance as the edge-to-edge distance between the NPs, and two of the model NP waveguides are shown in Figure 3. We also construct a NP chain where the NPs touch each other (d=0 Å). Note that we define particles to be touching each other when the center-to-center distance between two atoms from adjacent NPs is less than the Ag-Ag bond-forming distance (the Ag-Ag atom bond length is 3.00 Å). We would also like to point out that all of these chains are extremely large systems,
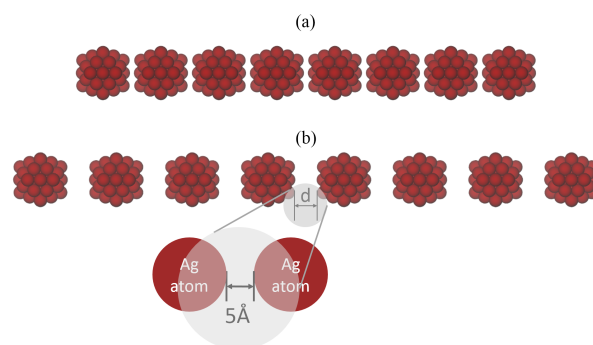

Fig. 3 Pictorial representation of two of the finite chains with 8 Ag NPs with radius a $\approx$ 1.23 nm and interparticle (edge-to-edge) distance equal to (a) 1 Å and (b) 5 Å.
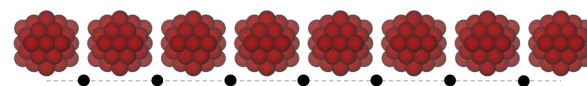

Fig. 4 The values of field intensity are taken at identical positions in each nanoparticle chain as shown by the black dots. The points lie exactly between two nanoparticles and on a line approximately 1 Å below the lowest atom in the NP.

each containing a total of 440 atoms. To simulate EET along the NP chains, we excite only the first Ag NP in the chain using a monochromatic laser with an energy equal to the plasmonic resonance energy of a single Ag NP (3.23 eV), and the entire system is allowed to evolve in time according to Eq. 6. To quantify the EET efficiency along the chain, we compute the electric field intensities, $I = \sqrt{\varepsilon_0/\mu_0} \times |E|^2$, where **E** is the total electric field, at identical points between each of the NPs along the axial direction shown in Figure 4, and ε_0 and μ_0 are the permittivity and permeability of free space, respectively. We utilize this metric of computing electric field intensities along the NP chain to allow for a direct comparison of EET efficiencies obtained in other previous studies.[9,31,32,55] Figure 5 shows the intensity trends of the NP chains with interparticle distances ranging from 0 to 5 Å. Transmission loss factors were calculated from Figure 5 by fitting to an exponential decay, $I = I_0 \ exp(-bz)$ with the transmission loss factor, b. The loss factors and decay lengths for all the chains are shown in Table 1. Table 1 also shows the group velocities for each of the chains (details on the calculation of group velocities are shown in the Supplementary Information). From the intensity trends in Figure 5 and transmission loss factors in Table 1, we observe a monotonic increase in the EET efficiency (i.e. the slope of the intensity lines and transmission loss factor both decrease) as the interparticle distance is reduced from 5 Å to about 2 Å. This result is in qualitative agreement with results obtained by previous studies on similar systems using classical electrodynamic methods.[32,55] This increase in EET efficiency can be attributed to an increase in capacitive coupling between the Ag NPs as the interparticle distance between them is reduced. This phenomenon is analogous to a charged capacitor,[56] where the capacitance of a capacitor increases as the charged plates are brought closer together. However, as the interparticle distance is further reduced
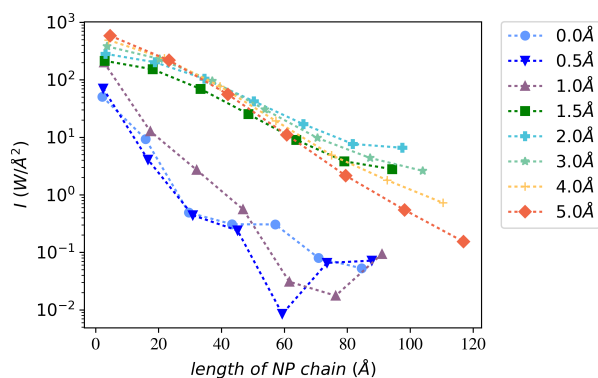
Fig. 5 Field intensities along silver NP chains with varying interparticle distances. The first nanoparticle in each of the chains is excited at the plasmon resonance energy, and the intensity values are computed at the interparticle gaps of the NPs as shown in Figure 3. The excitation energy used in the simulation is equal to the plasmon resonance energy of the single Ag nanoparticle. A drastic drop in the field intensity is seen for Ag chains with interparticle spacings less than 2 Å.

Fig. 6 Absorption spectrum for Ag NP dimers with varying interparticle separations. An additional lower-energy peak (corresponding to a charge transfer plasmon excitation) emerges in the absorption spectrum for dimers having an interparticle spacing less than 2 Å, denoted by red arrows.

below 2 Å, we observe an opposite trend of the EET efficiency. In particular, we see a sudden drop in EET efficiency for interparticle distances below 2 Å (i.e. the slope of the intensity line and transmission lost factor both increase). This result is qualitatively opposite to what has been predicted by previous computational studies.[32,55] Specifically, previous studies have observed a decrease in EET when the interparticle distance is reduced to a distance where the NPs directly touch each other.[55] In contrast, we observe a decrease in EET efficiency even before the instance when the NPs touch each other. At this point we would also like to mention that due to the finite nature of the chains, some end effects, such as the back transfer of electronic excitation energy, are seen in the shorter chains (interparticle spacings of 1 Å, 0.5 Å, and 0 Å). These end effects result in the non-monotonic intensity trends seen in the last few NPs and, hence, only a general trend of the chain is considered. A brief description of these end effects can be found in our previous study.[39]

Table 1 Transmission Loss Factor, Decay Length, and Group Velocity for the silver NP chains

Interparticle Distance (Å)	Transmission Loss Factor (1/Å)	Decay Length (Å)	Group Velocity (m/s (10^5))
5	0.057	17.54	2.341
4	0.048	20.83	2.570
3	0.041	24.39	2.802
2	0.035	28.57	3.295
1.5	0.038	26.32	2.937
1	0.186	5.38	1.775
0.5	0.199	5.03	1.523

Analyzing the electronic couplings in NP chains

We next investigate the decrease in EET efficiency by analyzing in detail the electronic couplings between the NPs in the plasmonic chain. For this purpose, we plot the absorption spectrum of Ag NP dimers with varying interparticle distances in Figure 6. On
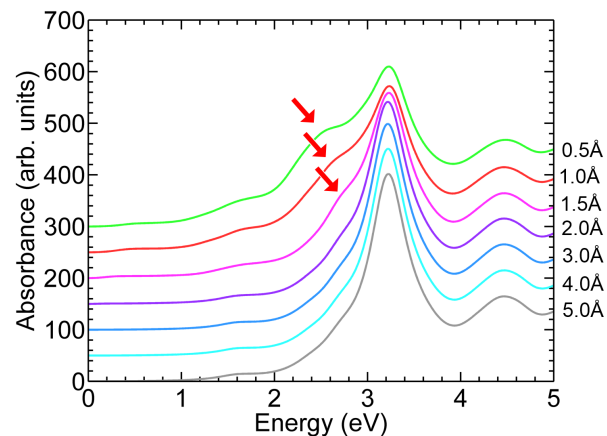
careful observation of Figure 6, we note that for all interparticle distances, a single prominent peak, close to the value of the single NP plasmonic energy is observed. However, for interparticle spacings less than 2 Å, an additional peak, at an energy lower than the prominent peak, forms in the absorption spectrum. This peak, marked with red arrows in Figure 6, is seen clearly in the absorption spectrum of the dimers with interparticle distances of 1, 0.5, and 0 Å. The prominent peak, close to the single NP plasmon energy, normally arises due to interactions (hybridizations) between the basic plasmon resonances of the elementary nanostructures (in this case, the single Ag NP). This excitation is the bonding (symmetric) mode, normally known as the Bonding Dipole Plasmon, or BDP, and is characterized by charge oscillations of the NPs in phase with each other.[21] The other peak appearing at lower energies and smaller interparticle distances, is normally observed when an optical-frequency conductive pathway is established between two NPs, enabling the transfer of charge between them. This conductive pathway can be physical, due to a physical bridge or due to quantum tunneling. This is known as a Charge Transfer Plasmon, or CTP.[22] Unlike the BDP, the CTP is characterized by a total charge moving between the two nanoparticles of the dimer, which we observe as the lower-energy peak in our absorption spectrum. In our case of non-touching NPs, the CTP excitation can be attributed completely to quantum tunneling that establishes a conductive pathway between the two NPs of the dimer. While charge transfer plasmons have been previously observed theoretically in DFT and quantum-corrected classical models,[22,30,56] to the best of our knowledge, this study is the first to predict CTPs using RT-TDDFTB calculations. The presence of a CTP peak is examined further below with our RT-TDDFTB calculations to understand the drop in EET efficiency.

Investigating the nature of plasmonic excitations

To analyze in detail the different plasmon modes and to assess changes in their nature, we need an intuitive way to analyze these
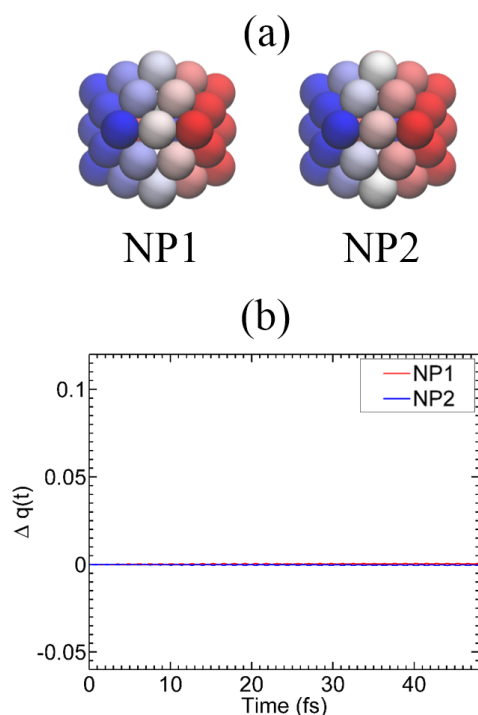
Fig. 7 (a) Snapshot of charge distributions at one time moment and (b) time-dependent total charge fluctuations at the BDP peak for a Ag NP dimer with interparticle distance equal to 5 Å. The charge distributions show a dipolar distribution of charges within each of the NPs. The time-dependent total charge oscillation shows no charge moving between the two NPs.

excitations. For example, the BDP is characterized by charge oscillations within individual NPs that are in phase with each other, while the CTP is characterized by the total charge oscillating from one NP to the other. Hence, we plot the Mulliken charge distribution in the 5 Å NP dimer at a single instance in time, excited at the BDP peak as shown in Figure 7(a). In particular, we observe a dipolar distribution of atomistic charges in each of the NPs that are in phase with each other. Furthermore, to get a quantitative picture of this particular excitation, we plot the changes in the Mulliken charges (Δq) for both NP1 and NP2, with respect to their ground state values as a function of time in Fig 7(b). In particular, we find that the time-dependent change in Mulliken charges in both the NPs remains constant with time. In conjunction with Figure 7(a), this shows that the charge oscillations only take place within individual NPs, confirming the BDP nature of the excitation. We now apply a similar analysis to a NP dimer, where the additional low-energy (CTP) peak appears. Figure 8 shows the charge distributions and the time-dependent changes in Mulliken charges for the NP dimer with an interparticle spacing of 1 Å. In this case, however, we compare the absorption spectra when the NP dimer is excited at either the BDP or CTP energy peak. When excited at the BDP peak, the 1 Å NP dimer shows charge distributions very similar to the charge distributions shown by the 5 Å dimer (Figure 8(b)), suggesting that it is a BDP-type excitation. However, the time-dependent changes in Mulliken charges shows

a rather different picture (Figure 8(d)), and we observe some charge transfer from one NP to the other. This is uncharacteristic of a BDP excitation, and we discuss this in detail later. Likewise, when excited at the CTP peak, one of the NPs shows a predominantly positive charge, while the other one shows a negative charge (Figure 8(a)). The time-dependent changes in Mulliken charges confirm this observation in Figure 8(c). This behavior is characteristic of a CTP excitation, where an oscillating current occurs between the two NPs of the dimer. A previous study[21] has similarly characterized CTP plasmons by plotting the charge distribution (at a single moment in time) and the electric current oscillating across a physical junction between two Ag dimers, at a frequency corresponding to the energy of this mode (i.e. the CTP mode). However, to the best of our knowledge, this study is the first to classify plasmonic excitations using time-dependent changes in Mulliken charges. We also note in Figure 8(a) that we observe a slight dipolar nature of charge distributions near the particle edges. This can be attributed to the atomistic treatment of the nanoparticles, whereby the charge transfer plasmon induced on the nanoparticle dimers also establishes a small opposing dipole on the inner edges of the same nanoparticles due to inter-atomic electrodynamic interactions. A previous study[25] has also observed a similar effect when they studied complex plasmonic clusters. Although this previous study investigated large plasmonic nanoparticles arranged in complex formations, the basic electrodynamics reasoning holds, even for our clusters.

The CTP-type behavior seen at the BDP peak (Figure 8(d)) confirms the previous hypothesis that the appearance of the CTP peak changes the nature of the original excitations in the dimer. In particular, we observe that at subnanometer interparticle spacings, the pure BDP excitation forms a hybridized excitation that has some CTP character. This hybridized BDP has also been called the screened BDP (S-BDP) or a higher-order charge transfer plasmon (CTP') in previous studies.[21,57] We attribute the decrease in the EET efficiency in smaller interparticle spacing chains to the formation of this hybridized BDP. Since the hybridized BDP allows for a small charge transfer between the NPs, it reduces the capacitive coupling between the NPs. Going back to the capacitor analogy used previously, this can be thought of as a leaking capacitor. Overall, the formation of such a hybridized BDP reduces the EET efficiency for subnanometer interparticle distances, unforeseen by classical models.

Conclusion

In summary, we utilize a real-time, time-dependent density functional tight-binding (RT-TDDFTB) approach to study, in atomistic detail, the electron dynamics of excitation energy transfer in large plasmonic nanoantenna systems. In particular, we study NP chains with subnanometer interparticle spacings that are beyond the capabilities of classical methods. Such systems are beyond the scope of classical methods such as FDTD and the FRET formalism due to the neglect of quantum effects (such as tunneling and hybridization) and beyond the routine use of conventional DFT due to size constraints. We also propose a visually intuitive way to classify the plasmonic resonances in nanoparticle systems, such as BDP, CTP, and hybridized excitations. Using the above
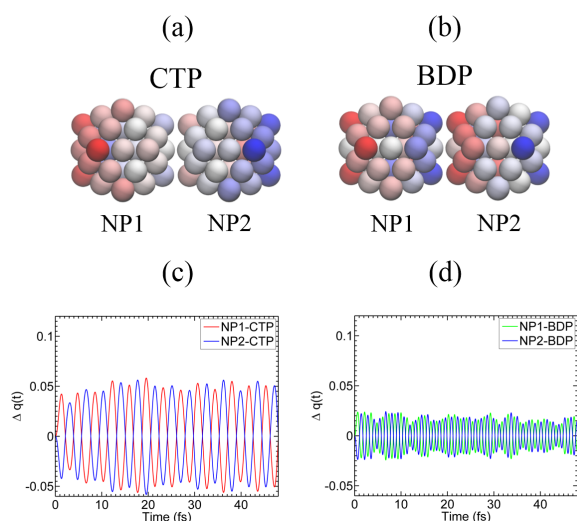
Fig. 8 Snapshot of charge distributions at one instance in time for a Ag NP dimer with an interparticle distance equal to 1 Å excited at (a) the CTP peak and (b) the BDP peak. The CTP peak distributions show a total charge separation between the two NPs, while the BDP peak distributions show dipolar charge distributions within each of the NPs. The time-dependent changes in Mulliken charges are shown for the (c) CTP and (d) BDP peak for the same Ag NP dimer. For both the CTP and the BDP excitations, a net charge fluctuation is seen between the NPs which indicates a hybridized nature of the BDP peak at subnanometer spacings.

methodologies, we find an initial monotonic increase in EET efficiency as the interparticle spacing in the chains is reduced, which is in qualitative agreement with classical studies. However, as the distance is further reduced we observe a drastic drop in EET efficiency. While classical electrodynamics methods have predicted this drop for NPs touching each other, our study shows this drop in efficiency occurs even before the NPs touch. We attribute this drop in efficiency to the interparticle charge transfer between the closely spaced nanoparticles. We further show that this charge transfer dramatically changes the nature of couplings between the nanoparticles in the chain. In particular, we demonstrate that the regular bonding dipole plasmon is converted to a hybridized bonding dipole plasmon, which possesses some charge transfer character. This, in turn, is ultimately responsible for the reduction in capacitive coupling between the NPs and hence the drop in EET efficiency. Consequently, our study has two important ramifications on EET in plasmonic nanosystems: (1) while classical methods based on solving Maxwell's equations have long been used to analyze a variety of nanoantenna systems, our findings show that the inclusion of quantum effects has a nontrivial effect on EET dynamics, especially in plasmonic nanoantennas with subnanometer interparticle spacings, and (2) decreasing the interparticle spacing beyond a certain limit may not have the intended effect of increasing EET efficiency and, therefore, a more careful consideration of other strategies may be necessary in improving energy transfer in plasmonic devices fabricated with subnanometer dimensions.

Conflicts of interest

There are no conflicts to declare.

Acknowledgements

Notes and references

1 A. Boltasseva and H. A. Atwater, *Science*, 2011, **331**, 290–291.
2 M. L. Brongersma and V. M. Shalaev, *Science*, 2010, **328**, 440–441.
3 C. M. Soukoulis and M. Wegener, *Science*, 2010, **330**, 1633–1634.
4 Y. A. Vlasov, M. O'Boyle, H. F. Hamann and S. J. McNab, *Nature*, 2005, **438**, 65–69.
5 C. F. Bohren and D. R. Huffman, *Absorption and scattering by a sphere*, Wiley Online Library, 1983.
6 S. A. Maier, P. G. Kik, H. A. Atwater, S. Meltzer, E. Harel, B. E. Koel and A. A. Requicha, *Nat. Mater.*, 2003, **2**, 229.
7 S. I. Bozhevolnyi, V. S. Volkov, E. Devaux, J. Y. Laluet and T. W. Ebbesen, *Nature*, 2006, **440**, 508–511.
8 L. Tong, R. R. Gattass, J. B. Ashcom, S. He, J. Lou, M. Shen, I. Maxwell and E. Mazur, *Nature*, 2003, **426**, 816–819.
9 D. Solis, A. Paul, J. Olson, L. S. Slaughter, P. Swanglap, W. S. Chang and S. Link, *Nano Lett.*, 2013, **13**, 4779–4784.
10 M. L. Brongersma, J. W. Hartman and H. A. Atwater, *Phys. Rev. B*, 2000, **62**, R16356.
11 S. Lal, S. Link and N. J. Halas, *Nat. Photonics*, 2007, **1**, 641.
12 G. D. Scholes, G. R. Fleming, A. Olaya-Castro and R. Van Grondelle, *Nat. Chem.*, 2011, **3**, 763.
13 S. J. Barrow, A. M. Funston, D. E. Gómez, T. J. Davis and P. Mulvaney, *Nano Lett.*, 2011, **11**, 4180–4187.
14 M. Moskovits, G. B. Braun, S. J. Lee, T. Laurence, N. Fera, L. Fabris, G. C. Bazan and N. O. Reich, *J. Phys. Chem. C*, 2009, **113**, 13622–13629.
15 W. S. Chang, L. S. Slaughter, B. P. Khanal, P. Manna, E. R. Zubarev and S. Link, *Nano Lett.*, 2009, **9**, 1152–1157.
16 E. Ozbay, *Science*, 2006, **311**, 189–193.
17 Y. Yin, Y. Lu, B. Gates and Y. Xia, *J. Am. Chem. Soc.*, 2001, **123**, 8718–8729.
18 Y. Cui, M. T. Björk, J. A. Liddle, C. Sönnichsen, B. Boussert and A. P. Alivisatos, *Nano Lett.*, 2004, **4**, 1093–1098.
19 S. Lin, M. Li, E. Dujardin, C. Girard and S. Mann, *Adv. Mater.*, 2005, **17**, 2553–2559.
20 M. G. Warner and J. E. Hutchison, *Nat. Mater.*, 2003, **2**, 272.
21 F. Wen, Y. Zhang, S. Gottheim, N. S. King, Y. Zhang, P. Nordlander and N. J. Halas, *ACS Nano*, 2015, **9**, 6428–6435.
22 W. Zhu, R. Esteban, A. G. Borisov, J. J. Baumberg, P. Nordlander, H. J. Lezec, J. Aizpurua and K. B. Crozier, *Nat. Commun.*, 2016, **7**, 11495.
23 M. Abb, P. Albella, J. Aizpurua and O. L. Muskens, *Nano Lett.*, 2011, **11**, 2457–2463.

24 N. Large, M. Abb, J. Aizpurua and O. L. Muskens, *Nano Lett.*, 2010, **10**, 1741–1746.

25 Y. Wang, Z. Li, K. Zhao, A. Sobhani, X. Zhu, Z. Fang and N. J. Halas, *Nanoscale*, 2013, **5**, 9897–9901.

26 A. Ahmadivand, B. Gerislioglu, R. Sinha, M. Karabiyik and N. Pala, *Sci. Rep.*, 2017, **7**, 42807.

27 P. Muehlschlegel, H.-J. Eisler, O. J. Martin, B. Hecht and D. Pohl, *Science*, 2005, **308**, 1607–1609.

28 P. Schuck, D. Fromm, A. Sundaramurthy, G. Kino and W. Moerner, *Phys. Rev. Lett.*, 2005, **94**, 017402.

29 S. Kim, J. Jin, Y.-J. Kim, I.-Y. Park, Y. Kim and S.-W. Kim, *Nature*, 2008, **453**, 757.

30 L. Wu, H. Duan, P. Bai, M. Bosman, J. K. W. Yang and E. P. Li, *ACS Nano*, 2012, **7**, 707–716.

31 D. Solis, B. Willingham, S. L. Nauert, L. S. Slaughter, J. Olson, P. Swanglap, A. Paul, W. S. Chang and S. Link, *Nano Lett.*, 2012, **12**, 1349–1353.

32 B. Willingham and S. Link, *Opt. Express*, 2011, **19**, 6450.

33 F. Wang, H. Liu, T. Li, S. Wang, S. Zhu, J. Zhu and W. Cao, *Appl. Phys. Lett.*, 2007, **91**, 133107.

34 I. Berlman, *Energy transfer parameters of aromatic compounds*, Elsevier, 2012.

35 E. Ploetz, E. Lerner, F. Husada, M. Roelfs, S. Chung, J. Hohlbein, S. Weiss and T. Cordes, *Sci. Rep.*, 2016, **6**, 33257.

36 V. A. Turek, M. P. Cecchini, J. Paget, A. R. Kucernak, A. A. Kornyshev and J. B. Edel, *ACS Nano*, 2012, **6**, 7789–7799.

37 G. Scholes, G. Scholes, X. Jordanides, X. Jordanides, G. Fleming and G. Fleming, *J. Phys. Chem. B*, 2001, **105**, 1640–1651.

38 S. Saini, G. Srinivas and B. Bagchi, *J. Phys. Chem. B*, 2009, **113**, 1817–32.

39 N. V. Ilawe, M. B. Oviedo and B. M. Wong, *J. Chem. Theory Comput.*, 2017, **13**, 3442–3454.

40 S. A. Maier, P. G. Kik and H. A. Atwater, *Phys. Rev. B*, 2003, **67**, 205402.

41 R. Esteban, A. G. Borisov, P. Nordlander and J. Aizpurua, *Nat. Commun.*, 2012, **3**, 825.

42 U. Hohenester, *Phys. Rev. B*, 2015, **91**, 205436.

43 M. B. Oviedo, C. F. A. Negre and C. G. Sánchez, *Phys. Chem. Chem. Phys.*, 2010, **12**, 6706.

44 M. B. Oviedo, X. Zarate, C. F. Negre, E. Schott, R. Arratia-Pérez and C. G. Sánchez, *J. Phys. Chem. Lett.*, 2012, **3**, 2548–2555.

45 C. F. A. Negre, V. C. Fuertes, M. B. Oviedo, F. Y. Oliva and C. G. Sánchez, *J. Phys. Chem. C*, 2012, **116**, 14748–14753.

46 M. B. Oviedo and B. M. Wong, *J. Chem. Theory Comput.*, 2016, **12**, 1862–1871.

47 M. Elstner, D. Porezag, G. Jungnickel, J. Elsner, M. Haugk, T. Frauenheim, S. Suhai and G. Seifert, *Phys. Rev. B*, 1998, **58**, 7260–7268.

48 T. Frauenheim, G. Seifert, M. Elstner, Z. Hajnal, G. Jungnickel, D. Porezag, S. Suhai and R. Scholz, *Phys. Status Solidi B*, 2000, **217**, 41–62.

49 R. G. Parr and R. G. Pearson, *J. Am. Chem. Soc.*, 1983, **105**, 7512–7516.

50 S. Mukamel, *Principles of nonlinear optical spectroscopy*, Oxford University Press on Demand, 1999.

51 B. Aradi, B. Hourahine and T. Frauenheim, *J. Phys. Chem. A*, 2007, **111**, 5678–5684.

52 J. Ma, Z. Wang and L.-W. Wang, *Nat. Commun.*, 2015, **6**, 10107.

53 T. Lünskens, P. Heister, M. Thämer, C. A. Walenta, A. Kartouzian and U. Heiz, *Phys. Chem. Chem. Phys.*, 2015, **17**, 17541–17544.

54 C. F. Negre, E. M. Perassi, E. A. Coronado and C. G. Sánchez, *J Phys Condens Matter*, 2013, **25**, 125304.

55 M. Quinten, A. Leitner, J. R. Krenn and F. R. Aussenegg, *Opt. Lett.*, 1998, **23**, 1331.

56 L. Wu, S. F. Tan, M. Bosman, J. K. Yang, C. A. Nijhuis and P. Bai, *RSC Adv.*, 2016, **6**, 70884–70894.

57 J. A. Scholl, A. García-Etxarri, A. L. Koh and J. A. Dionne, *Nano Lett.*, 2013, **13**, 564–569.